A Numerical Investigation of Laser Heating Including the Phase Change Process in Relation to Laser Drilling

I.Z. Naqavi, E. Savory, R.J. Martinuzzi

The Univ. of Western Ontario, Dept. of Mech. And Materials Engg.

London, Ontario, Canada. N6A 5B9

A laser is an intense source of heat and finds wide application in the materials processing industry. When a metallic surface is irradiated with a laser, a large temperature gradient is produced in the near surface region and, for high-energy lasers, temperatures up to the melting or even the boiling temperature of the material may be reached. Whenever the boiling temperature is reached on the surface, it starts to ablate and a hole is created. Modeling of the laser heating process enhances the understanding of the physical processes involved and provides the guidelines for the control of the process. Laser heating of steel is considered here. The heating process is modeled with a Fourier heating model and a phase change process is included in it. The governing equations are solved numerically. In the case of drilling the shape of the domain continually changes and so the numerical scheme is employed in such a way as to incorporate this change. Moreover, a physically realistic boundary condition is considered at the ablating surface. In this study the profile of the drilled hole and its progress with time is predicted. The evolution of the temperature field in the substrate material is also investigated.

1. INTRODUCTION

A laser provides an intense source of heat, and such devices are widely used in industry for machining of metallic substrates. The laser usually provides very precise machining operations and produces a fusion zone with high depth-width ratios, which minimizes the total amount of material affected or distorted by the laser beam. The amount of energy absorbed by the substrate material is very high which causes very high surface temperatures. In some cases this temperature can be as high as the boiling point of the material. When the substrate reaches boiling point material starts to eject as gas or vapour from the surface and the surface recedes towards the substrate bulk. In the case of high-energy, short pulse, laser heating, with pulse lengths of the order of nanoseconds or less, gas or vapour ejection from the surface dominates over the melting process and the liquid layer formed between the vapour and solid phases is negligibly small. For such a thin layer of liquid and for such a small duration, the Marangoni effect is not important and vapour or gas ejection becomes the dominant mechanism forming the cavity. High-intensity, short-pulse laser heating is mainly used in drilling and shock processing through surface ablation.

The laser short-pulse heating process with vapour or gas ejection from the surface has been studied extensively. An analytical solution of short-pulse laser heating was obtained by Yilbas [1] with an evaporative boundary condition at the surface. He used the Laplace transformation method to solve the governing heat conduction equation. Modest and Abakians [2] modeled the evaporative cutting of a semi-infinite solid with a moving continuous wave (c.w.) laser. They solved the simplified non-linear governing equations

2

numerically and obtained the laser produced groove depth and shape for various laser and material properties. Basu and Date [3] investigated the laser melting of a metallic substrate with the Marangoni effect. They solved the momentum and heat transfer equations to evaluate the flow field in the melt pool. They used the incident laser beam as a surface heat source and did not consider any vapour or gas ejection from the surface. Wei and Ho [4] investigated the drilling process. They found that the shape of the vapour-liquid and liquid-solid interface and the hole penetration velocity was dependent on the energy distribution and the power of the beam.

When a laser irradiates a surface some part of the beam is reflected. In the case of a flat surface the reflected part is simply a waste of energy but in the case of drilled hole cavities there could be multiple reflections inside the cavity, which affects the shape and size of the drilled hole. Bang and Modest [5] studied these multiple reflections during the laser cutting process. They divided the groove surface into triangular elements, with linear interpolation for local irradiation calculations. They found that the multiple reflections caused higher material removal rates and larger grooves. Moreover, the cavity profile became flatter near beam centreline and acquired steep slopes in other parts. Ganesh et.al. [6,7] modeled the transient developments in a laser drilled hole. They considered the conduction and advection heat transfer in solid and liquid metal. In their model they included the free surface flow of the melt and its expulsion from the cavity. They used the SOLA-VOF (SOLution Algorithm-Volume of Flow) method to track the solid-liquid and liquid-vapour interfaces.

In the present work, high intensity laser pulse heating of the order of few nanoseconds is considered. For a stationary laser beam an axi-symmetric heating model is employed. To account for phase changes i.e. solid-liquid and liquid-gas transformations, a modified heat transfer model is used. In particular, this new model can deal with the liquid-gas phase change and can track the receding surface of the drilled hole. The laser beam is considered as a step pulse with a Gaussian energy distribution across the heated surface. Here we are only concerned with initial hole formation in semi-infinite substrate material.

2. MATHEMATICAL ANALYSIS OF THE LASER HEATING PROCESS

In this study the laser induced heating and phase-change is modeled using the energy method. The present form of the energy method is able to handle the liquid-gas phase-change. The following assumptions are made in order to model the laser induced heating, with subsequent phase change, in a metallic solid:

- The substrate material and laser are both stationary. This gives rise to axisymmetric heating, as shown in Fig 1.

- The substrate is isotropic and so constant material properties are considered.

- The material has a certain absorption depth for the laser radiation. Moreover, the solid and liquid phases have the same absorption coefficient during the phase change process.

- A laser beam is absorbed by the liquid or solid phases, thereby generating a heat source.

- The laser beam intensity has a Gaussian distribution.

4

- Heat losses due to radiation or convection from the surface or the generated cavity are omitted, since they are negligibly smaller when compared to the internal energy gain of the substrate material. This will result in an insulated boundary condition.

- The substrate material is a pure substance with single melting and evaporation temperatures.

- When the solid starts ablating the resulting gas does not interact with the laser beam and the liquid-gas interface starts moving inside the substrate material with a certain recession velocity, creating a cavity.

- There is no ionization of the emerging gas front.

- Inside the formed cavity there are no multiple reflection phenomena and it is assumed that there is negligible or zero reflectance from the surface of the cavity.

- The vapour region has no interaction with the substrate material.

- There is no re-condensation of the vapours in the cavity.

In the analysis, the laser beam has its spot centre at the centre of the co-ordinate system. In the case of simple heating of the solid or liquid phase, the heat conduction equation is valid. When the temperature reaches the phase change temperatures of the substrate material (melting and boiling temperatures) during the heating process, the phase change is considered i.e. the melting and subsequent ablation of the solid substrate are introduced in the governing equation of heat transport, with appropriate boundary conditions. The transient heat transfer equation for a solid substrate irradiated by a laser beam is written as:

$$\rho c_p \frac{\partial T}{\partial t} = \frac{k}{r} \frac{\partial}{\partial r} \left(r \frac{\partial T}{\partial r} \right) + k \frac{\partial^2 T}{\partial z^2} + S_o \tag{1}$$

where, for a step input pulse,

$$S_o = I_o \delta (1 - r_f) \exp(-\delta z) \exp\left(-\frac{r^2}{a^2} \right) \tag{2}$$

Here ρ is the density, c_p is the specific heat, k is the thermal conductivity, T is the temperature of the substrate material, I_o is the beam power intensity, δ is the absorption depth parameter, r_f is the surface reflectivity and a is the Gaussian parameter.

The initial condition is:

$$T = T_o \quad (specified) \quad at \quad t = 0 \quad (initially) \tag{3}$$

The boundary conditions are:

$$\frac{\partial T}{\partial z} = 0 \quad at \quad z = 0 \quad (surface) \tag{4}$$

$$\frac{\partial T}{\partial r} = 0 \quad at \quad r = 0 \quad (axis\ of\ symmetry) \tag{5}$$

$$T = T_o \quad at \quad r, z \to \infty \quad (specified) \tag{6}$$

When the temperature reaches the phase change temperature melting or boiling starts. It is assumed that the substrate material has single melting and boiling temperatures, i.e. when the substrate material reaches the melting or boiling temperature, the phase change takes place at a constant temperature. In the Stefan problem the phase change is assumed to occur at a sharp interface between two phases. However, to capture this interface in a

numerical solution is quite difficult. We are assuming here that, instead of a sharp interface, the phase change takes place over quite a wide region called the "mushy zone". The mushy zone consists of a mixture of partially solid and partially liquid phases, in the case of a solid-liquid phase change, or partially liquid and partially gas phases for the liquid-gas phase change (Figs 1 & 2). Now, to formulate the energy transport equation in this mushy zone, consider a differential element within it. Let the differential element be subjected to the melting process and x_m be the mass fraction of the liquid present in the element. The energy content i.e. the enthalpy ΔU of the differential element with volume ΔV at the melting temperature T_m can be written as:

ΔU = Latent Heat of Liquid + Sensible Heat of Liquid + Sensible Heat of Solid

$$\Delta U = m_m L_m + m_m c_{pm} \left(T_m - T_{ref} \right) + m_s c_p \left(T_m - T_{ref} \right) \qquad (8)$$

where,

$$x_m = \frac{m_m}{m_m + m_s} \qquad (9)$$

T_{ref} is the reference temperature for calculating enthalpy, T_m is the melting point temperature, L_m is the latent heat of fusion, c_{pm} is the specific heat of the melt, m_m is the mass of liquid and m_s is the mass of solid in the element. It is assumed that the density ρ of the solid and liquid phase at T_m is the same. In that case

$$m_m = \rho \Delta V x_m$$

$$m_s = \rho \Delta V \left(1 - x_m \right)$$

Inserting these values in equation (8) gives,

$$\Delta U = \rho \Delta V \left[x_m \left(L_m + c_{pm} \left(T_m - T_{ref} \right) \right) + c_p \left(1 - x_m \right) \left(T_m - T_{ref} \right) \right]$$ (10)

On further assuming that the specific heat of the melt is same as a solid at the melting

temperature $\left(c_{pm} = c_p \ \ at \ \ T = T_m \right)$, equation (10) reduces to,

$$\Delta U = \rho \Delta V \left[x_m L_m + c_p \left(T_m - T_{ref} \right) \right]$$

For a unit volume, it reduces to:

$$\frac{\Delta U}{\Delta V} = \Delta u = \rho \left[x_m L_m + c_p \left(T_m - T_{ref} \right) \right]$$

Differentiation with time yields:

$$\frac{\partial u}{\partial t} = \rho L_m \frac{\partial x_m}{\partial t}$$ (11)

since $c_p \left(T_m - T_{ref} \right) = const.$

It is important to note that in the conduction equation (1) $\rho c_p T$ is also the enthalpy per

unit volume i.e.

$$\rho c_p \frac{\partial T}{\partial t} = \frac{\partial u}{\partial t}$$ (12)

Using equations (11) and (12) and substituting into equation (1) gives the energy

equation for the differential element subjected to the phase change process, i.e. melting,

as:

$$\rho L_m \frac{\partial x_m}{\partial t} = \frac{k}{r} \frac{\partial}{\partial r} \left(r \frac{\partial T}{\partial r} \right) + k \frac{\partial^2 T}{\partial z^2} + S_o$$ (13)

Equation (13) is applicable to the differential elements (cells defined by nodes in the

substrate material) when the temperature reaches the melting temperature of the substrate

material $(T = T_m)$ and $0 \leq x_m \leq 1$, i.e. in a mushy zone. Consequently, here the temperature of the cells with $0 \leq x_m \leq 1$ is set to the melting temperature $(T = T_m)$. When the value of x_m exceeds 1 $(x_m > 1)$ equation (13) is no longer applicable for the differential element under consideration because the phase change process has been completed for that element and it is no longer in the mushy region. In this case, equation (1) is used to determine the temperature change in the liquid phase i.e. the liquid heating initiates and continues until the temperature reaches the boiling temperature of the substrate material. It is important to note that inside the mushy region terms like $\dfrac{\partial T}{\partial r}$ and $\dfrac{\partial T}{\partial z}$ are zero because the temperature is constant. However, equation (13) is valid at the mushy zone/solid and mushy zone/liquid interfaces where these terms are not zero in general.

In the case of the temperature reaching the boiling temperature, the mushy zone consideration needs to be implemented again. In this case, equation (13) can be modified for a differential element, which is subjected to the boiling, i.e.:

$$\rho L_b \frac{\partial x_b}{\partial t} = \frac{k}{r} \frac{\partial}{\partial r} \left(r \frac{\partial T}{\partial r} \right) + k \frac{\partial^2 T}{\partial z^2} + S_o \tag{14}$$

Here L_b is the latent heat of boiling or evaporation and x_b is the mass fraction of the gas or vapour present in the boiling differential element. The material starts ablating from the surface elements subjected to boiling. In that case, an appropriate boundary condition is needed at the boiling surface region. Since the boiling process occurs at a constant

temperature, it is reasonable to assume that the temperature at the ablating surface is equal to the boiling temperature and so this is the boundary condition, i.e.

$$T = T_b \quad at \ \ z = z_b, r = r_b \tag{15}$$

where z_b and r_b represent the axial and radial locations at the ablating surface. When ablation starts material will be removed from the surface and the surface will recede to form a cavity. Thus z_b and r_b will keep changing with time and so are also part of the solution. In the numerical algorithm a technique will be discussed to use equation (14) to track this receding surface.

3. NUMERICAL SOLUTION

The governing equations used to model this phase change process are a set of three energy equations (1), (13) and (14). To obtain the temperature field in the substrate material these equations are solved numerically. Equation (1) is applicable to solid and liquid heating, equation (13) is applicable to the mushy zone at the solid-liquid interface and equation (14) is applicable to the mushy zone at the liquid-gas (or vapour) interface. A finite volume approach [8] is used to discretize these equations. Since the equations are modeling an unsteady process, the discretized equations are solved explicitly. From the initial conditions a temperature field is calculated for the next time step. If any cell reaches the melting or boiling temperature, the discretized counterpart of equation (13) or (14) is used to determine whether that cell is in the mushy zone or not.

If, for any cell, equation (13) gives $0 \leq x_m \leq 1$, the cell is lying in the solid-liquid mushy zone, and $T = T_m$. Similarly, if equation (14) gives $0 \leq x_b \leq 1$, the cell is lying in the liquid-gas mushy zone, and $T = T_b$.

As shown in Fig 1, equation (13) will also be applicable at some points on the boundaries. For those cases the same boundary conditions are applicable as for equation (1). For equation (14) the boundary condition is defined in equation (15). As mentioned earlier, equation (14) is also used to track the receding surface. Fig 1 shows that, for this particular problem, equation (14) is applicable only on the cells near the surface. If, for any cell, $x_b = 1$, i.e. in that particular cell all the liquid has been changed to gas and escaped from the surface, that cell will no longer be part of the domain and the boundaries have to be shifted to the adjacent cells in the zone.

Since all these calculations are being performed in an explicit manner, stability analysis [8] shows that;

$$\left(\frac{2k}{\rho c_p \Delta r^2} + \frac{2k}{\rho c_p \Delta z^2} \right) \Delta t \leq 1 \tag{16}$$

Where Δr and Δz are the grid size in radial and axial direction respectively. The computational domain is divided into a grid and a grid independence test was performed for different grid sizes and distribution, resulting in a non-uniform grid with 200×200 grid points. In this set-up (Fig 3) a finer grid is used near the surface and near the axis of symmetry, the regions where most of the energy is concentrated. The grid becomes

11

coarser as it moves towards the bulk of the substrate material. The time increment, based on stability criteria (16), using the finest grid is calculated as 8×10^{-13} seconds. A computer program was developed to implement this scheme for calculating the temperature field and hole geometry.

4. RESULTS AND DISCUSSION

Using the numerical scheme described in the previous section, the laser heating and subsequent phase change is simulated for a step input pulse. Here steel is considered as the substrate material and its properties are given in Table 1, whilst the laser beam properties are given in Table 2.

Fig 4 shows the temperature variation on the surface at the beam spot centre with time. The temperature starts to increase with heating, but at time $t = 0.136 ns$ it stops increasing. At this particular time the corresponding temperature is T_m which shows that the melting process has started. Once melting has been completed, the liquid heating takes over and the temperature starts to increase again. This temperature variation is shown to continue up to the time $t = 0.3 ns$. After this, boiling commences, material starts to eject from the surface and the surface starts to recede towards the bulk of the substrate.

Temperature variations along the surface (Fig 5) and along the axial direction (Fig 6) show the heating pattern during the drilling process. In Figure 5 the curves do not start from $r = 0$ but, rather, at some distance from the symmetry axis. Since material starts to

12

eject from the surface in the very early stages of heating, by $t = 2ns$ there is a large crater on the surface. As the heating proceeds, with time the size of the crater on the surface increases and this pushes the temperature curves farther away from the symmetry axis. However, the distance between the curves decreases which shows that expansion of the crater is slowing down. In this case, the beam has a Gaussian intensity distribution and beyond the point where the beam intensity is less than $\left(\frac{1}{e}\right)$ times the peak intensity (Fig 3) there is not enough energy available to ablate the material from the surface. This limit defines the radial dimension of the drilled hole. One important feature of short pulse heating is the high temperature gradient. In the radial direction the temperature changes from $3000\ ^oC$ to almost room temperature within a distance of only $2 \times 10^{-4}\,m$, giving a temperature gradient of the order of $10^7\ ^oC/m$. There are two distinct regions on the temperature curves. The region above $1800\ ^oC$ shows the liquid heating, whilst the lower part is the solid heating. The two regions are separated by a bump on the curve around $1800\ ^oC$ that corresponds to the mushy zone at the solid-liquid interface. The temperature variation along the symmetry axis shows an almost similar behaviour to its radial counterpart. One obvious difference is the way in which the curves shift away from the surface. Because of the material removal, the surface recedes towards the bulk of the material. Here, unlike the radial variation, the distance between the curves does not change which shows that near the symmetry axis the material removal rate and surface recession is uniform and does not slow down with time. Unlike the radial direction, when the depth of the cavity increases in the axial direction, the newly exposed material receives the same amount of energy as the old surface, which causes the same removal rate to occur. Another difference between the radial and axial temperature variations is

the temperature gradient. In the axial direction the temperature gradient is even higher, of the order of 10^9.

In short pulse laser heating a high amount of localized energy is deposited in the substrate material. In the early heating period, a high-energy deposition rate results in a sharp temperature rise in the vicinity of the surface and the bulk of the substrate remains at a relatively lower temperature. Because of such a short duration, the energy cannot diffuse in the bulk of the material. As the heating proceeds, it would be expected that diffusion should take over. However, once the surface temperature reaches boiling point, material starts to eject from the surface and so at each time step a new surface is exposed to the laser beam. This process holds the diffusional effects in check, whilst the phase change and material removal consume the better part of the energy deposited.

The curves in Fig 7 show the surface of the drilled hole. These curves represent surface of revolution. The cavity surface development is in accord with the discussion for the temperature variation in the substrate. In the early heating period, the cavity development in the radial direction is fast but it slows down as it reaches the $\left(\frac{1}{e}\right)$ point of the beam intensity (Fig 3). On the other hand, in the axial direction the cavity keeps extending. This results in the walls of the drilled hole becoming steeper, whilst near the base of the hole the surface acquires a sharper curvature.

Figs 8 and 9 show the temperature contours inside the substrate material at 4 and 8 nanoseconds, respectively. The energy deposition rate is $7 \times 10^{12}\ W/m^2$, with a pulse length of 8 ns. This typical contour shape arises from the surface ablation and the cavity formation in the substrate material. As described previously, the cavity does not expand much in the radial direction but the change in the axial direction is very prominent. The contour plots show that although these contours are moving as the surface ablation is progressing, they do not really penetrate into the substrate material. This indicates that there is insufficient diffusion taking place such that the heat does not conduct toward the bulk of the substrate. In a very thin region near the surface, energy is absorbed and this immediately raises the temperature. Before any heat diffusion can take place, the temperature reaches the boiling point and material starts to eject from the surface. Thus, most of the energy deposited in short pulse heating is used in cavity formation rather than in heating of the bulk of the substrate. The contours with temperatures above $1800\ ^oC$ represent the very thin liquid phase layer developed in the cavity.

Unlike conventional drilling processes, laser drilling relies on phase change and for this purpose the substrate is brought to temperatures far beyond the re-crystallization temperature. Laser drilling can produce a very large heat affected zone where the material properties may differ from the bulk of the substrate.

To see the effect of the laser parameters, namely the beam intensity and pulse length, on the development of the heat affected zone, simulations are performed for different pulse

15

lengths and beam intensities. Since a wide range of laser beam intensity and energies are available, arbitrary values may be chosen. In this study these parameters are adjusted such that almost the same depth of drilled hole is achieved as for the 8 ns pulse. Figs 10, 11, 12 show temperature contours for beams with pulse lengths of 6, 4 and 2 ns and beam intensities of 9.3×10^{12}, 14×10^{12} and 28×10^{12} $W/_{m^2}$, respectively. It appears from these contours that with decreasing pulse length and increasing beam intensity, the depth of the heat-affected zone reduces considerably. Fig 13 shows the temperature variation along the axial direction for various beam intensities, confirming the fact that the temperature decreases at a much faster rate along the axial direction with increasing intensity, as was also observed from the temperature contours. The temperature at the surface of the cavity is in the vicinity of the boiling temperature for all the beam intensities studied. Moving a short distance away towards the bulk of the material the temperature difference at any given point for different beam intensities could be significant, e.g. at the depth of $1.18 \times 10^{-6} m$ temperatures for 28×10^{12} $W/_{m^2}$ and 7×10^{12} $W/_{m^2}$ beams are 1810 $^{\circ}C$ and 2390 $^{\circ}C$, respectively. This observation confirms the energy interaction picture described previously. When the energy deposition rate increases, the rate of temperature rise in the surface vicinity increases as well. With negligible heat diffusion toward the bulk of the material, the surface starts evaporating. Fig 14 shows the variation of the temperature gradient along the axial direction for various beam intensities. Since the temperature at the surface is the boiling temperature of the material and it decreases rapidly as we move away from the surface, it results in very large temperature gradients. Here, it is obvious that with an increase in the beam intensity the peak temperature gradient value also increases. It has been shown in previous work [9] that large

temperature gradients in laser heating result in very large thermal stresses in the substrate material. But, interestingly, here the large thermal gradient generated with increasing beam intensity is confined to the liquid phase and in the solid phase the temperature gradients are not very much different for different beam intensities. Hence, it may be expected that different beam intensities will generate almost identical stress fields.

It is interesting to note from Figs 8 and 9 that the pulse length has no effect on the size of the heat-affected zone. With a longer pulse a deeper drilled hole is achieved, although the depth of the heat-affected zone remains same. Indeed, the depth of the heat-affected zone is more dependent on the energy deposition rate.

5. CONCLUSIONS

In this study a laser heating process with phase change is modeled. To model the phase changes involved in the process the concept of a "mushy zone" is introduced and an appropriate form of the energy equations is derived for the solid-liquid and liquid-gas mushy zones. These model equations are solved numerically to obtain the temperature field and the shape of the drilled hole. The following conclusions are derived from this work:

1. The model described in this study captures the phase change process in laser heating.

2. There is a high temperature gradient generated in the vicinity of the surface. With a high-energy deposition rate, material ejection from the surface overcomes the diffusion of energy to the bulk of the substrate.

3. The drilled hole expands in the axial direction at a steady rate but the expansion in the radial direction is limited because of the radial energy distribution in the beam.

4. The depth of the heat-affected zone in the substrate material is independent of pulse length, whereas it can be reduced by using a larger pulse intensity.

6. REFERENCES

[1] Yilbas, B. S., Analytical solution for time unsteady laser pulse heating of semi-infinite solid, Int. J. Mech. Sci., **39**(6), 1997, 671-682.

[2] Modest, M. F. and Abakians, H., Evaporative cutting of a semi-infinite body with a moving cw laser, Trans. ASME, J. Heat Transfer, **108**, 1988, 602-607.

[3] Basu, B. and Date, A. W., Numerical study of steady state and transient laser melting problems-I. Characteristics of flow field and heat transfer, Int. J. Heat and Mass Transfer, **33**, 1990, 1149-1163.

[4] Wei, P. S. and Ho, J. Y., Energy considerations in high energy beam drilling, Int. J. Heat and Mass Transfer, **33**(10), 1990, 2207-2217.

[5] Bang, S. Y. and Modest, M. F., Multiple reflection effects on evaporative cutting with a moving cw laser, Trans. ASME, J. Heat Transfer, **113**, 1991, 663-669.

[6] Ganesh, R. K., Faghri, A. and Hahn, Y., A generalized thermal modeling for laser drilling process-I. Mathematical modeling and numerical methodology, Int. J. Heat and Mass Transfer, **40**(14), 1997, 3351-3360.

[7] Ganesh, R. K., Faghri, A. and Hahn, Y., A generalized thermal modeling for laser drilling process-II. Numerical simulation and results, Int. J. Heat and Mass Transfer, **40**(14), 1997, 3361-3373.

[8] Patanker, S. V., Numerical Heat Transfer and Fluid Flow, Hemisphere Publishing Corp., 1980.

[9] Yilbas, B.S. and Naqavi I.Z., Laser heating including the phase change process and thermal stress generation in relation to drilling, Proc. Instn. Mech. Engrs. Part B J. Engineering Manufacture,Vol. 217, 2003, 977-991.

Thermal conductivity $k \; \left(W \middle/ mK \right)$	Specific heat $c_p \; \left(J \middle/ kgK \right)$	Density $\rho \; \left(kg \middle/ m^3 \right)$	Latent heat of fusion $L_m \; \left(J \middle/ kg \right)$
52	330	7836	2.4×10^5
Latent heat of boiling $L_b \; \left(J \middle/ kg \right)$	Melting temperature $T_m \; (K)$		Boiling temperature $T_b \; (K)$
6.26×10^6	1810		3030

Table 1: Material properties for steel.

Pulse intensity $I_o \; \left(W \middle/ m^2 \right)$	Absorption depth parameter $\delta \; \left(1 \middle/ m \right)$	Gaussian parameter $a \; (m)$	Heating period (ns)
7, 9.3, 14 & $28 \left(\times 10^{12} \right)$	6.16×10^6	3.06×10^{-4}	8, 6, 4 & 2

Table 2: Properties of the laser beam
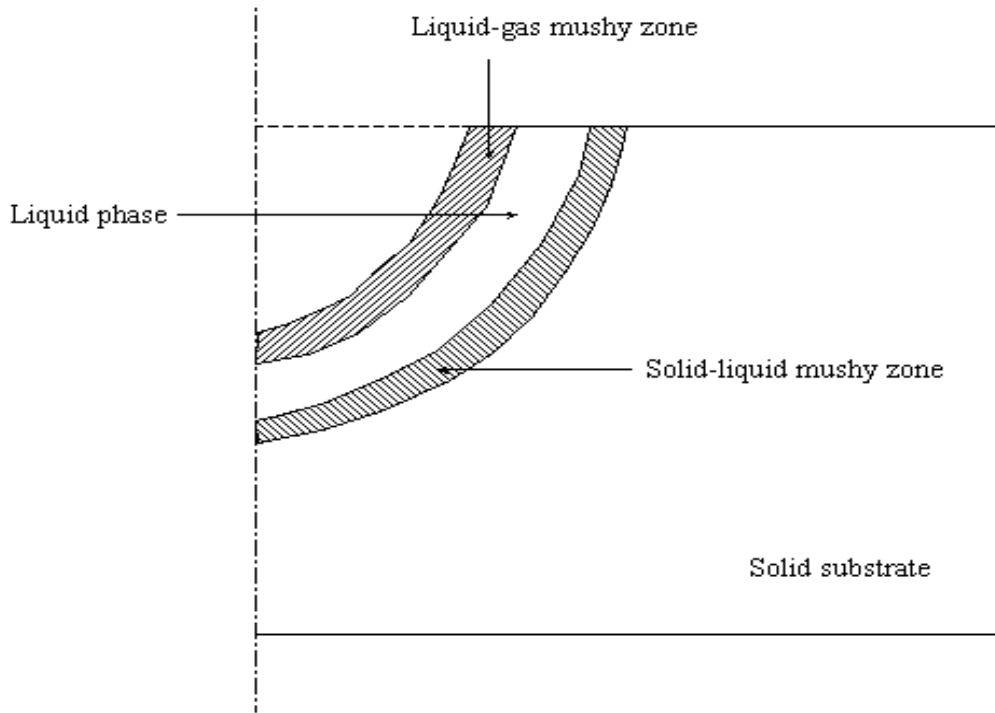
Figure 1: Axisymmetric heating and surface ablation with two mushy zones.
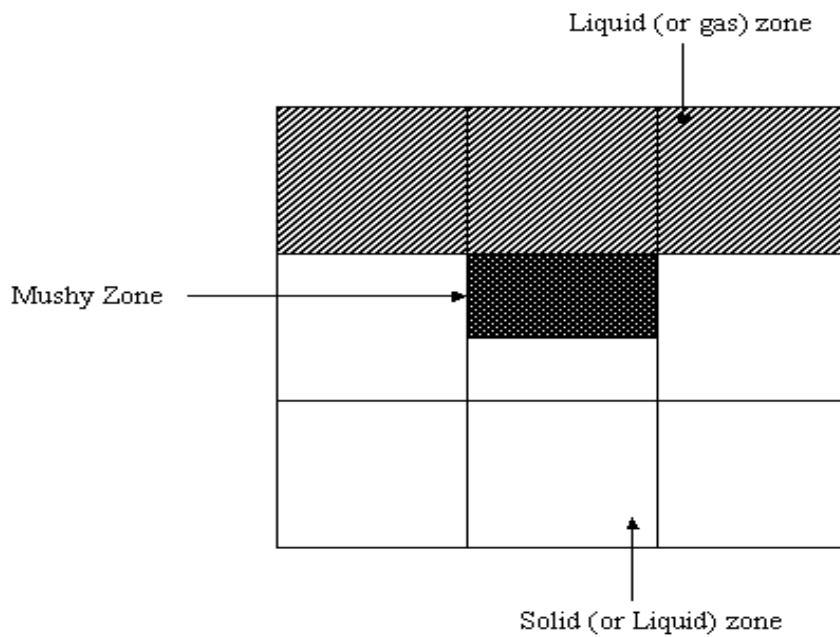
Figure 2: Schematic view of the mushy cell.
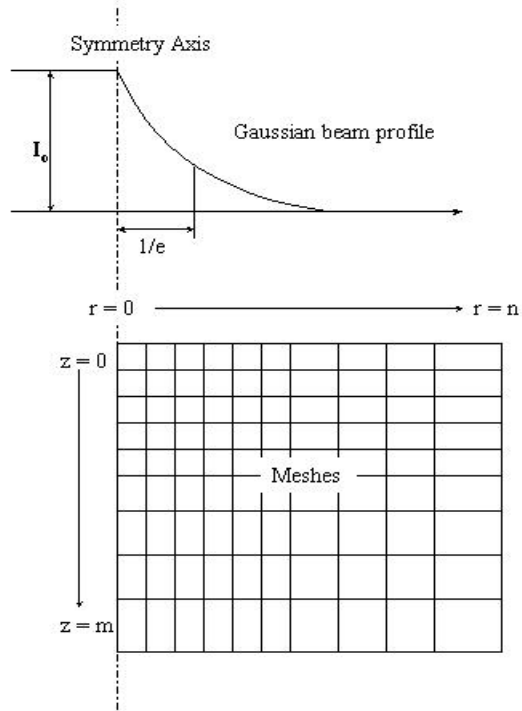
Figure 3: Gaussian beam profile and numerical grid in the physical domain.
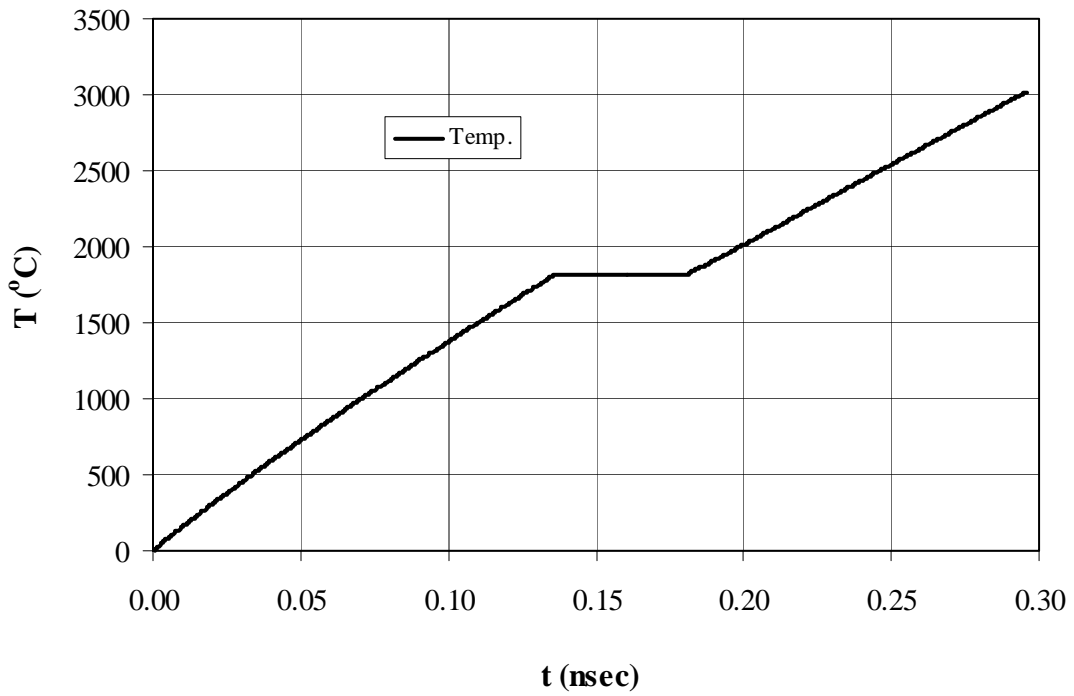
Figure 4: Temporal variation of temperature at the beam centre with step input pulse.
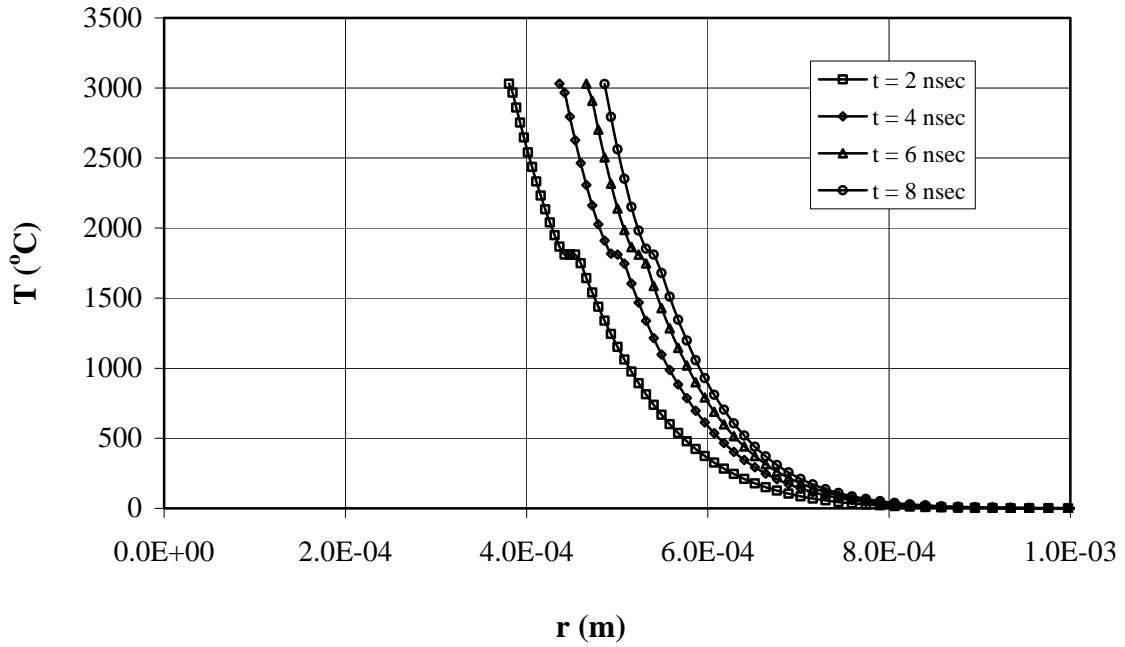
Figure 5: Spatial temperature variation along the surface.
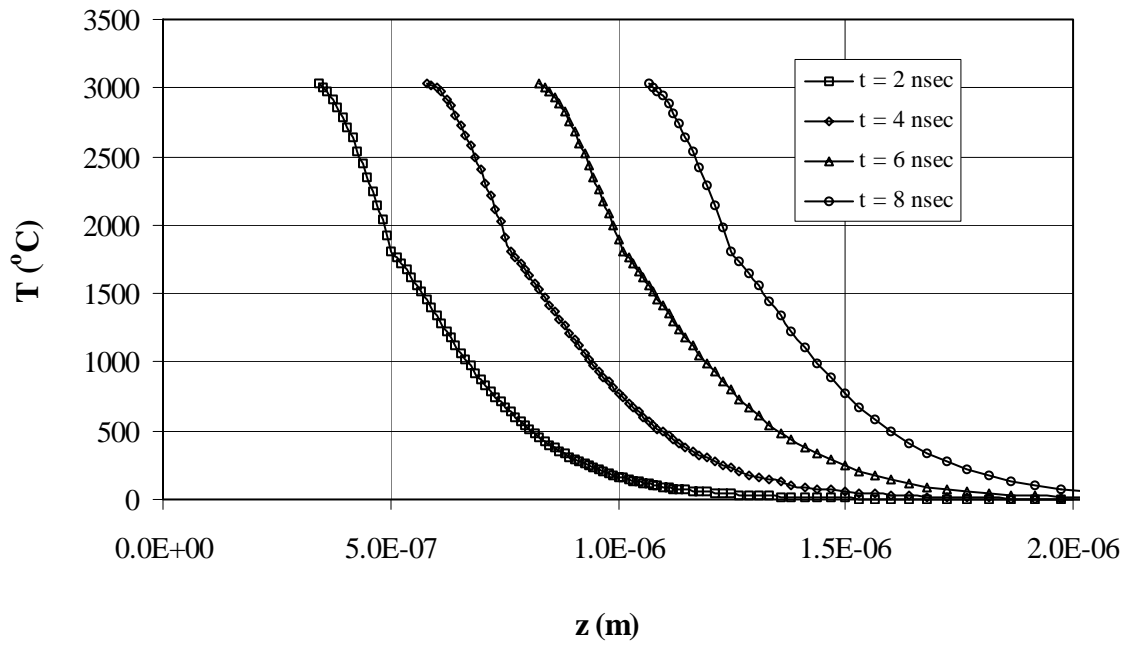
Figure 6: Spatial temperature variation along the axial direction.
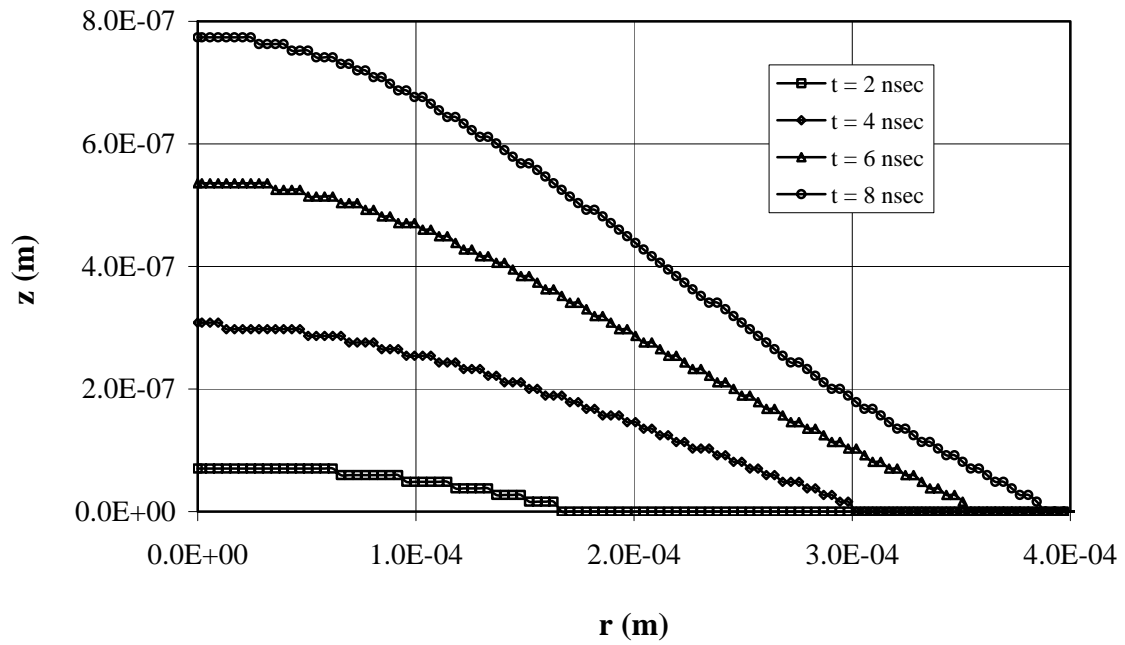
Figure 7: *Development of the drilled hole geometry.*
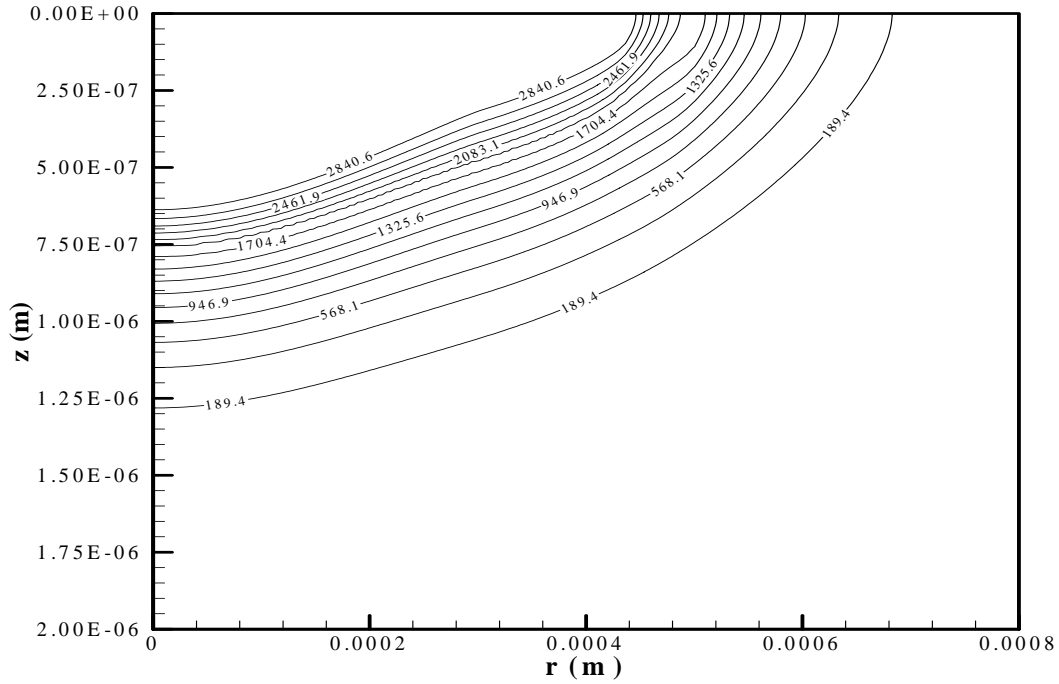
Figure 8: Temperature contours in the substrate at 4 ns with pulse intensity of $7 \times 10^{12} \, W/m^2$.
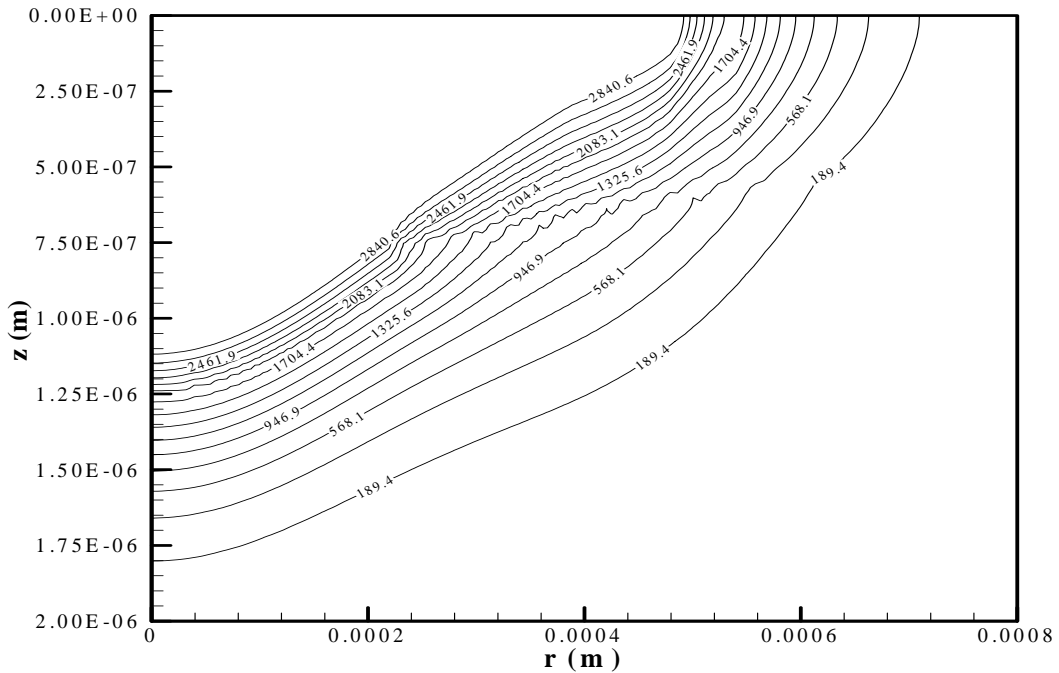
Figure 9: Temperature contours in the substrate at 8 ns with pulse intensity of $7 \times 10^{12} \, W/m^2$.
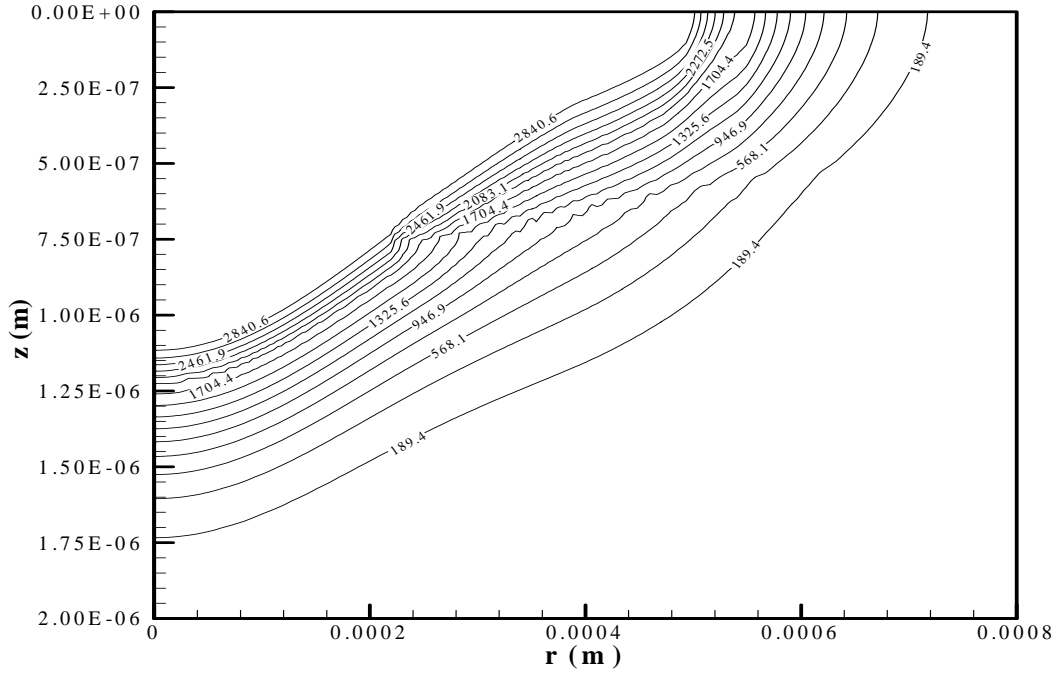
Figure 10: *Temperature contours in the substrate at 6 ns with pulse intensity of* $9.3 \times 10^{12} \, W/m^2$.
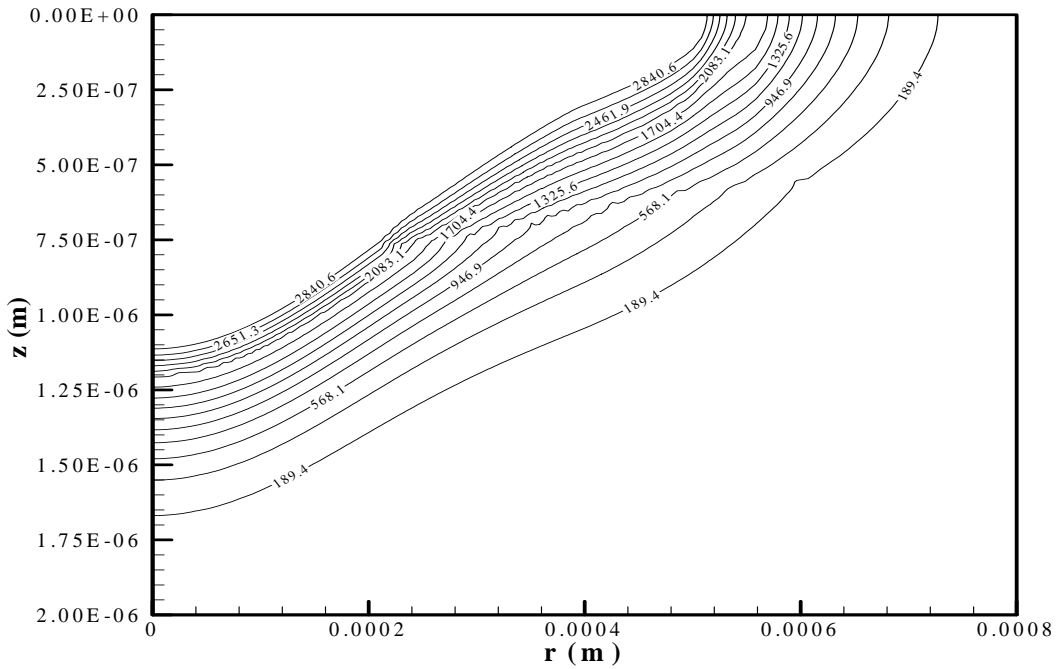
Figure 11: *Temperature contours in the substrate at 4 ns with pulse intensity of* $14 \times 10^{12} \, W/m^2$.
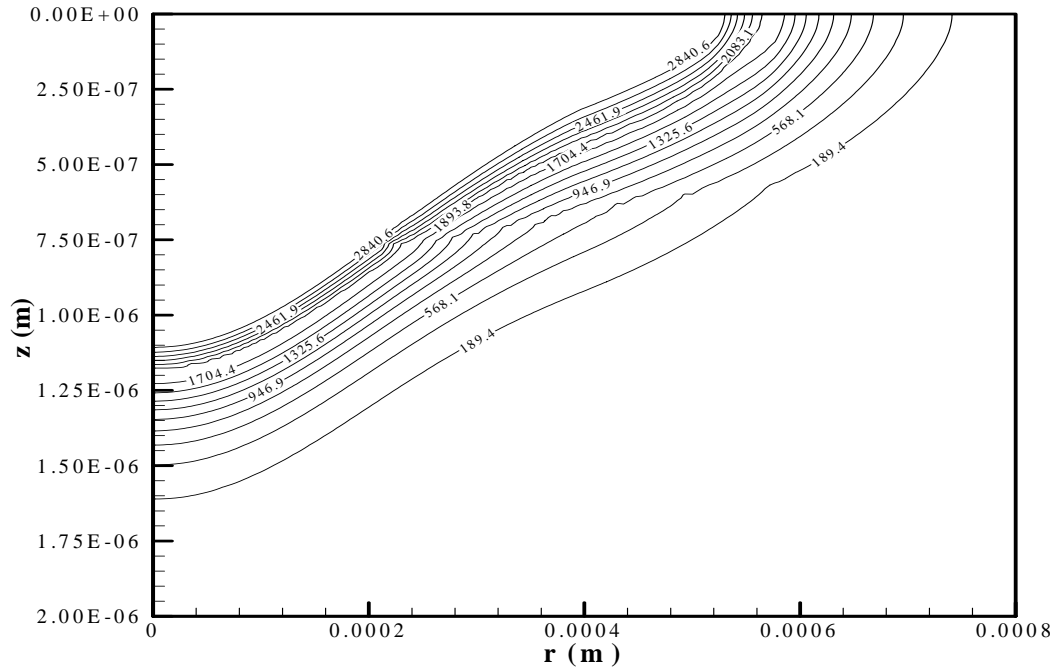
Figure 12: *Temperature contours in the substrate at 2 ns with the pulse intensity of* $28 \times 10^{12} \, W/m^2$ *.*
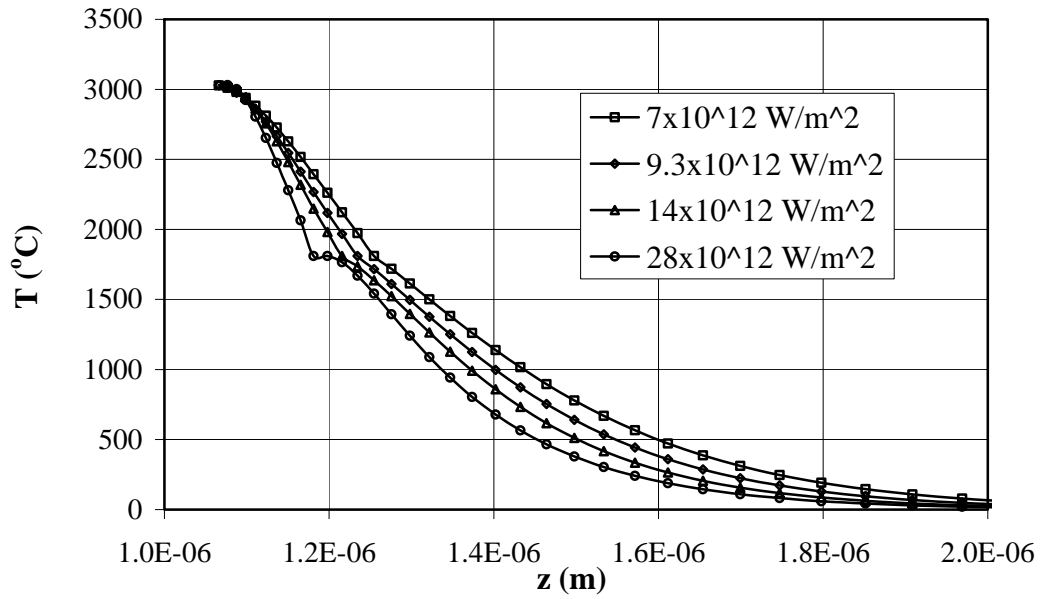
Figure 13: *Spatial temperature variation along axial direction for different beam intensities.*
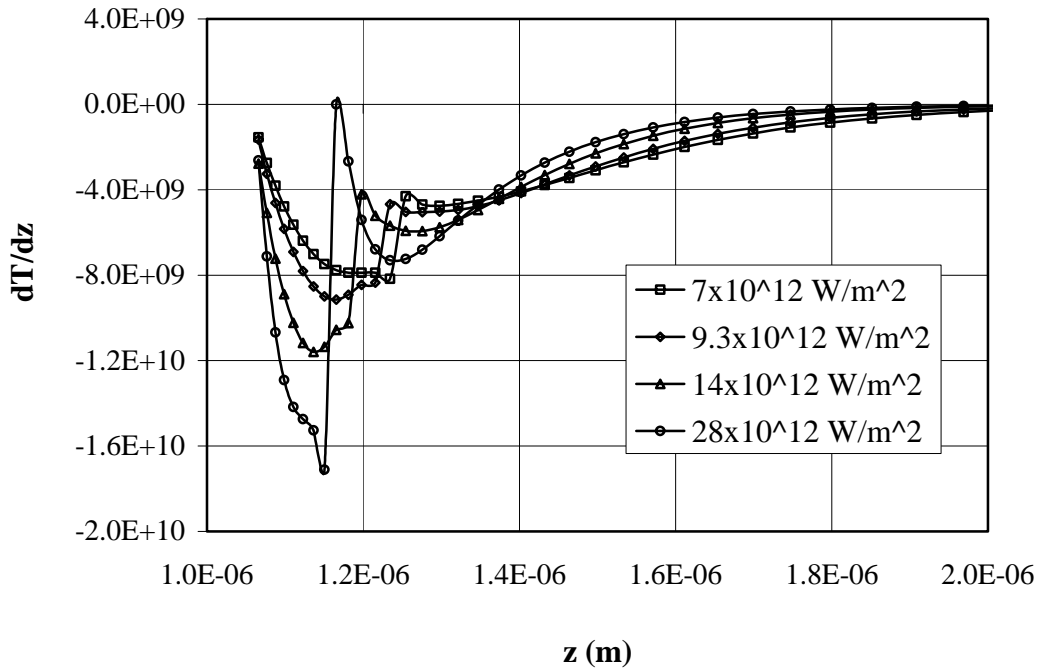
Figure 14: *Spatial temperature gradient variation along axial direction for different beam intensities.*